Electron Transport in Single-Wall Carbon Nanotube Weak Links in the Fabry-Perot Regime

H. I. Jørgensen,[1,*] K. Grove-Rasmussen,[1] T. Novotný,[1,2] K. Flensberg,[1] and P. E. Lindelof[1]

[1]*Nano-Science Center, Niels Bohr Institute, University of Copenhagen, Universitetsparken 5, DK-2100 Copenhagen Ø, Denmark*

[2]*Department of Electronic Structures, Faculty of Mathematics and Physics, Charles University, Ke Karlovu 5, 121 16 Prague, Czech Republic*

(Received 21 October 2005; published 25 May 2006)

We fabricated reproducible high transparency superconducting contacts consisting of superconducting Ti/Al/Ti trilayers to gated single-wall carbon nanotubes. The reported semiconducting single-wall carbon nanotubes have normal state differential conductance up to $3e^2/h$ and exhibit clear Fabry-Perot interference patterns in the bias spectroscopy plot. We observed subharmonic gap structure in the differential conductance and a distinct peak in the conductance at zero bias, which is interpreted as a manifestation of the supercurrent. The gate dependence of this supercurrent as well as the excess current are examined and compared to the coherent theory of superconducting quantum point contacts with good agreement.

DOI: 10.1103/PhysRevLett.96.207003 PACS numbers: 74.45.+c, 73.23.Ad, 73.63.Fg, 74.50.+r

Electron transport through a single-wall carbon nanotube (SWCNT) bridging two metal electrodes has been studied intensively over the past years. At low temperatures, different transport regimes depending on the transparency of the metal-SWCNT interfaces have been identified. With low transparency contacts, a quantum dot (QD) will be defined in the SWCNT [1–4], and, with intermediate transparency contacts, Kondo resonances around zero bias are observed [5,6]. High transparency contacts were in recent years also reported, where the SWCNT constitutes an electron waveguide with Fabry-Perot (FP) interferences [7,8].

Changing the metal electrodes to superconductors (S) dramatically changes the transport characteristics. In such junctions, the carbon nanotube (CNT) forms a weak link between the two superconductors, and several interesting effects can be observed. At zero bias, a supercurrent can flow through the weak link [9–11] due to the Josephson effect [12], while at low biases current will be carried by multiple Andreev reflections (MARs) at the two CNT-S interfaces [13–15]. For large bias, these effects will give rise to an excess current.

In fact, only very recently have these effects been seen in SWCNT devices [9] similar to the one presented here. In this Letter, we present transport measurements on a gated S-SWCNT-S Josephson junction at low temperatures, with high transparency contacts. We focus on the gate dependence of the excess current and zero-bias conductance peak in the FP regime.

The SWCNTs are grown by chemical vapor deposition (CVD) from catalyst islands made by electron beam lithography and positioned relative to predefined alignment marks. The details of the CVD-growth procedure are described elsewhere [16,17]. After growth, source and drain electrodes consisting of superconducting trilayers are positioned next to the catalyst islands to contact the SWCNT. The gap between the source and drain trilayer films is approximately 500 nm. The superconducting trilayers consist of 5 nm titanium to make good contact to the SWCNT, then of 40 nm aluminum to raise the transition temperature, and finally 5 nm titanium to stop oxidation of the aluminum.

Our devices are made on a highly doped silicon wafer with a 0.5 μm thermally oxidized SiO_2 layer on top. We use the silicon substrate as a back gate. To be able to measure the transition temperature T_C and the critical field B_C of the trilayer films at low temperatures, we furthermore define a four probe device of the superconducting trilayer. For the device in this Letter, we find $T_C = 750$ mK, $B_C = 75$ mT, and from BCS theory we calculate a superconducting energy gap of $2\Delta \simeq 3.5k_BT_C = 230$ μeV. However, the actual effective value of Δ for the CNT weak link might differ from this measured value due to interface effects, and, indeed, we found from the fit of the excess current measurements (see below) that the effective gap is reduced by about a factor of $\sim$0.7. All measurements are preformed at 300 mK in a sorption pumped ^{3}He cryostat (Oxford Instruments Heliox). The measurements are made with standard digital to analog converter cards, lock-in amplifiers (excitation 5 μV), and optocouplers to reduce noise.

Figure 1 shows a gate sweep from -10 to 0 V with $V_{sd} = 1$ mV$(>2\Delta/e)$. It displays strong gate dependence: high conductance at high negative gate voltages and low conductance at small gate voltages, which indicates that the SWCNT is semiconducting. The SWCNT defines a QD with gate dependent Schottky barriers at each interface. The gate thus tunes both the energy levels of the QD and the strength of the Schottky barriers.

From $V_{gate} \sim -4$ V to $V_{gate} \sim -2$ V, the Schottky barriers are large and the SWCNT constitutes a closed QD; i.e., the charging energy U_C is larger than the broadening of the energy levels Γ. Transport is dominated here by charging effects, and Coulomb blockade peaks are clearly

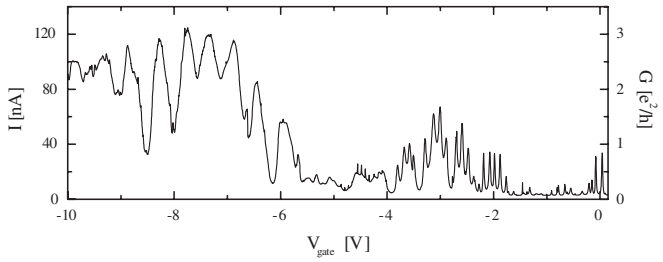

FIG. 1. Current and conductance for the S-SWCNT-S Josephson junction as a function of voltage applied to the back gate with 1 mV source-drain voltage. The high conductance regime with Fabry-Perot oscillations is reached at large negative gate voltages ($<-$ 6 V). Coulomb blockade peaks are seen at lower gate voltages.

visible. Some of the peaks are spaced into periods of four due to the fourfold degeneracy (spin and orbital) of each energy level, also confirmed by bias spectroscopy plots (not shown). Such characteristics are a sign of a high quality SWCNT. As the gate voltage is decreased to more negative values, the Schottky barriers are decreased, leading to an increase of Γ. Below $V_{\text{gate}} \sim -5$ V, the dot opens, Γ becomes larger than U_C, and charging effects of the QD are no longer dominant. Instead, the FP interference of the electron waves being reflected at the SWCNT-electrode interfaces dominates transport.

Figure 2(a) shows a bias spectroscopy plot in this gate region with a small magnetic field applied ($B = 100$ mT) to suppress the superconducting state of the electrodes. The average differential conductance in this gate region is around $\sim 2.5e^2/h$ with maximums of about $\sim 3e^2/h$, approaching the theoretical limit of $4e^2/h = (6.5\ \text{k}\Omega)^{-1}$. The maximum value of $\sim 3e^2/h$ of the conductance implies a rather large asymmetry $\Gamma_L/\Gamma_R = 3$ of the CNT couplings to the contacts (found from a resonant level model representing the system well around a conductance peak), in contrast to fairly symmetric couplings reported elsewhere [9,14]. As V_{gate} and V_{sd} are changed, the dips in conductance evolve into straight lines, forming a mesh of crossing dark lines. These pronounced oscillations in differential conductance versus V_{gate} and V_{sd} are clear signs of the FP interferences [7]. In the FP region, we estimate $\Gamma = \Gamma_L + \Gamma_R \sim 2$ meV by fitting the resonances in Fig. 2(a) with a Lorentzian line shape, and the level spacing $\Delta E \sim$ 4–7 meV as half of the distance in source-drain voltage between two resonances.

As we turn off the magnetic field, i.e., turn on the superconducting state of the electrodes, an overall increase in differential conductance between $V_{\text{sd}} \sim \pm 2\Delta/e$ is observed [Fig. 2(b)]. A more detailed bias spectroscopy plot of this overall increase through two successive resonances is shown in Fig. 2(c). Detailed measurements with a lock-in amplifier of differential conductance versus V_{sd} at gate voltages indicated in Fig. 2(c) are shown in Figs. 3(a) and 3(b), where Fig. 3(a) is a cut through a resonance and Fig. 3(b) is a cut through an antiresonance. A characteristic

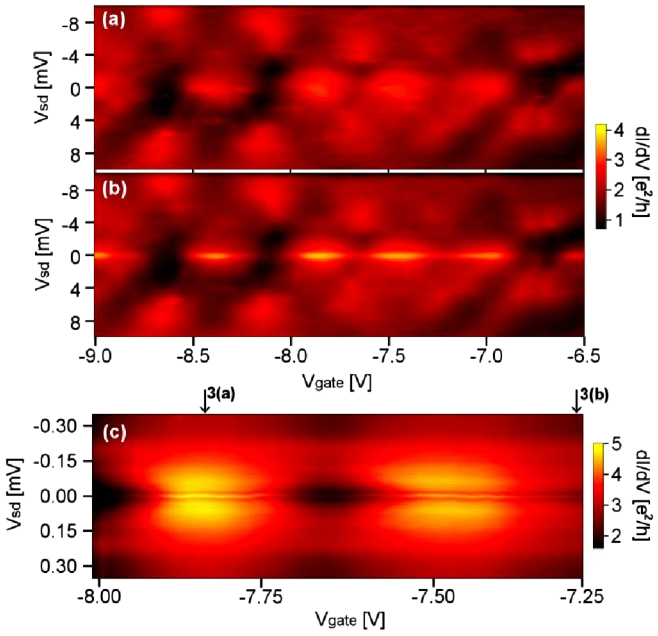

FIG. 2 (color online). (a) Bias spectroscopy plot in the high transparency gate region, with a small magnetic field ($B =$ 100 mT) to suppress the superconducting state of the electrodes. (b) Analogous to (a) but without magnetic field, i.e., with superconducting electrodes. (c) Close-up on two of the resonances from which the excess current and supercurrent of Fig. 4 are extracted. Arrows are pointing to the gate voltages where the graphs in Figs. 3(a) and 3(b) are measured.

conductance variation between $V_{\text{sd}} \sim \pm 2\Delta/e$ is seen for all gate voltages. Close to $|V_{\text{sd}}| \sim 2\Delta/e$, the conductance starts to increase, while at smaller source-drain voltages a dip centered around zero bias also develops. In Fig. 3(b), this dip can be seen between $V_{\text{sd}} \sim \pm 80\ \mu$V and less strongly in Fig. 3(a). The change in conductance between $V_{\text{sd}} \sim \pm 2\Delta/e$ to typically higher, but sometimes also lower, values than the normal state differential conductance G_N is because superconductivity induced transport mechanisms occur.

Between $V_{\text{sd}} \sim \pm 2\Delta/e$, transport is governed by Andreev reflections (ARs) [18] and normal reflections.

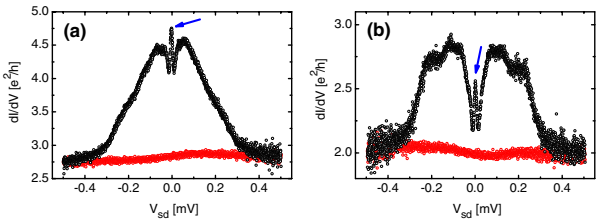

FIG. 3 (color online). Differential conductance versus source-drain voltage measured with a lock-in amplifier (5 μV excitation) at different gate voltages as indicated in Fig. 2(c). The upper curve (black) is for the superconducting electrodes, and the lower curve (red) is with the magnetic field of 100 mT to suppress the superconductivity of the electrodes. (a) is measured at a resonance of the Fabry-Perot pattern, while (b) is measured at an antiresonance. Blue arrows point to the supercurrent peak.

An electron with energy $|\epsilon| < \Delta$ relative to the Fermi energy in the normal region has (depending on the barrier strength) a probability for being an AR on the superconductor as a hole effectively transferring two electrons (one Cooper pair) through the SWCNT-S interface [19,20]. For $|\epsilon| > \Delta$, ARs are still possible but fall off rapidly. Multiple Andreev reflections between the two superconducting leads at finite bias give rise to a subgap structure (SGS) [21–24], while at zero bias a dissipationless supercurrent can flow providing that the interfaces are sufficiently transparent. In Fig. 3(b), we observe features for $|V_{sd}| \lesssim 2\Delta/e$ and a distinct peak around zero bias, which is a general trend in our S-SWCNT-S junctions with high transparency. At $|V_{sd}| \gg 2\Delta/e$, transport is mostly due to quasiparticle transport, and the FP pattern is seen in Fig. 2(b). As we approach $|V_{sd}| \sim 2\Delta/e$ from above, the quasiparticle transport is enhanced due to the modified density of states of the superconductors, and below this point the SGS is expected to appear. We observe a complex pattern in the subgap region for the lower transparency case [Fig. 3(b)], while the higher transparency one [Fig. 3(a)] does not show much structure, in qualitative agreement with theoretical predictions [24,25]. The structure in Fig. 3(b) seems too smeared to allow for quantitative comparison with theory, yet it is an interesting subject for further studies.

Instead of studying in detail the SGS, we focused on its integral effect in the form of the excess current I_{exc}, which is defined as the difference in current between having the electrodes in the superconducting state and the normal state at $V_{sd} \gg \Delta/e$. It can therefore be found as half of the difference in area between the two set of data points in Figs. 3(a) and 3(b). In Fig. 4(a), we have extracted the excess currents from the bias spectroscopy plot in Fig. 2(c) and plotted them as functions of the normal state differential conductance. Since the level width is much larger than the superconducting gap, $\Gamma_{L,R} \gg \Delta$ (see above), we can use for the interpretation of the results the well-established theory of superconducting quantum point contacts [25,26] and fit the excess current with the function

$$I_{exc}(g) = \frac{e\tilde{\Delta} g^2}{h(4-g)}\left[1 - \frac{g^2}{4\sqrt{4-g}(8-g)} \times \log\frac{2+\sqrt{4-g}}{2-\sqrt{4-g}}\right], \quad (1)$$

where g is the conductance measured in units of e^2/h and where $\tilde{\Delta}$ is the gap parameter at the S-SWCNT interface. Allowing for renormalization of $\tilde{\Delta}$ and performing a least-square fit to the measured data, we get $\tilde{\Delta} \sim 0.7\Delta$. Using this value in Eq. (1) yields the curve in Fig. 4(a) and also the data points in Fig. 4(d), showing good agreement between experiments and the theoretically extracted excess current.

Next, we discuss the zero-bias anomaly that we observe for all gate voltages in the FP region. The peak has a full width of only $\sim 25\ \mu$V (see Fig. 3). Such a peak in conductance at zero bias was observed earlier [14,15] and was attributed to a dissipative quasiparticle current [27]. In this work, however, we pursue an alternative interpretation, viewing the peak as a manifestation of the supercurrent. We interpret half of the area of the zero-bias peak (*not* the whole area *under* the peak) as a measure of the supercurrent. At first glance, this interpretation seems inconsistent, since the measured peak area is of the order of 0.2 nA, while the expected magnitude of the supercurrent is on the order of $2e\tilde{\Delta}/\hbar \sim 35$ nA, i.e., more than 2 orders of magnitude higher. However, a similar discrepancy between the measured and expected values of the supercurrent has been observed previously [9,28]. In particular, in a very recent study [9] on a similar device to ours, where the supercurrent was measured as zero-bias current, a discrepancy

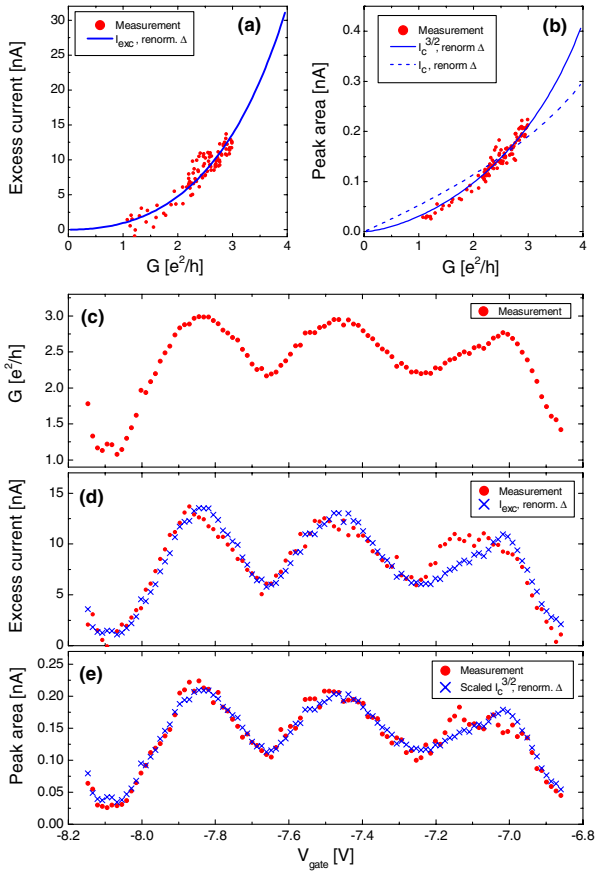

FIG. 4 (color online). Comparison between measured and theoretical data. (a) Measured (dots) and fitted (line) excess current as a function of conductance ($G = ge^2/h$). The fitted line is calculated from Eq. (1) using $\tilde{\Delta}$ as a fitting parameter. (b) Measured (dots) and fitted (lines) supercurrent. The fits are to $a(I_c)^{3/2}$ (solid line) and aI_c (dashed line), using a as a fitting parameter; see text for discussion. (c) Measured conductance in the Fabry-Perot regime as a function of gate voltage. (d) Measured (dots) and calculated (crosses) excess current. (e) The zero-bias anomaly area measured (dots) and calculated (crosses). The theoretical points (crosses) in (d) and (e) are calculated using the measured conductance in (c) and Eqs. (1) and (2), respectively.

of the order of 15 between the measured and expected values was found. The suppression can be understood in terms of the dynamics of the superconducting phase of a resistively and capacitively shunted Josephson junction with the environment, resulting in an apparent critical current I_m scaling as $I_m \propto I_c^{3/2}$, with I_c being the bare critical value of the supercurrent I_c; see Refs. [9,28] for details [29].

Adopting this idea, we perform a fit to the measured zero-bias-peak area as a function of the normal state conductance [Fig. 4(b)]. The supercurrent is determined as [24,26]

$$I_c(g) = \frac{e\tilde{\Delta} g \sin\varphi_{\max}}{4\hbar\sqrt{1-\frac{g}{4}\sin^2(\frac{\varphi_{\max}}{2})}} \tanh\frac{\tilde{\Delta}\sqrt{1-\frac{g}{4}\sin^2(\frac{\varphi_{\max}}{2})}}{2k_BT}, \quad (2)$$

where $\varphi_{\max}$ is the phase at which the supercurrent in Eq. (2) is maximal. Using the renormalized value of the gap, we have fitted the data to both $aI_c(g)$ and $aI_c^{3/2}(g)$, with a being a fitting parameter. We clearly see that the conductance dependence of $I_c^{3/2}(g)$ fits the measured data very well. On the other hand, the dependence of $I_c(g)$ does not fit the data at all, comparable with analogous results of Ref. [9]. The resulting V_{gate} dependence of the peak area is plotted in Fig. 4(e) using the fitted values of $I_c^{3/2}(g)$ with $\tilde{\Delta}$. Thus, we conclude that the zero-bias-peak results are fully consistent with the theoretical predictions based on the supercurrent interpretation.

In conclusion, we have successfully fabricated gated S-SWCNT-S Josephson junctions with high transparency contacts. In the Fabry-Perot regime of the semiconducting SWCNT reported here, we observed enhanced current due to MARs for $|V_{\text{sd}}| < 2\Delta/e$ and a conductance peak around zero bias. We interpret the zero-bias conductance peak as a not fully developed supercurrent. The excess current, which has not been analyzed before for such junctions, fits very well to the theory for coherent superconducting quantum point contacts.

We acknowledge the support of the Danish Technical Research Council (The Nanomagnetism framework program), EU-STREP Ultra-1D program, and the Nano-Science Center, University of Copenhagen, Denmark. The work of T. N. is a part of the research plan MSM 0021620834 that is financed by the Ministry of Education of the Czech Republic.

*Electronic address: hij@fys.ku.dk

[1] S. Tans, M. H. Devoret, H. Dai, A. Thess, R. E. Smalley, L. J. Geerligs, and C. Dekker, Nature (London) **386**, 474 (1997).

[2] M. Bockrath, D. H. Cobden, P. L. McEuen, N. G. Chopra, A. Zettl, A. Thess, and R. E. Smalley, Science **275**, 1922 (1997).

[3] D. H. Cobden and J. Nygård, Phys. Rev. Lett. **89**, 046803 (2002).

[4] P. J. Herrero, S. Sapmaz, C. D. L. P. Kouwenhoven, and H. S. van der Zant, Nature (London) **429**, 389 (2004).

[5] J. Nygård, D. H. Cobden, and P. E. Lindelof, Nature (London) **408**, 342 (2000).

[6] B. Babic, T. Kontos, and C. Schönenberger, Phys. Rev. B **70**, 235419 (2004).

[7] W. Liang, M. Bockarth, D. Bozovic, J. H. Hafner, M. Tinkham, and H. Park, Nature (London) **411**, 665 (2001).

[8] J. Cao, Q. Wang, M. Rolandi, and H. Dai, Phys. Rev. Lett. **93**, 216803 (2004).

[9] P. Jarillo-Herrero, J. A. van Dam, and L. P. Kouwenhoven, Nature (London) **439**, 953 (2006).

[10] J. Haruyama, K. Takazawa, S. Miyadai, A. Takeda, N. Hori, I. Takesue, Y. Kanda, N. Sugiyama, T. Akazaki, and H. Takayanagi, Phys. Rev. B **68**, 165420 (2003).

[11] A. Y. Kasumov, R. Deblock, M. Kociak, B. Reulet, H. Bouchiat, I. I. Khodos, Y. B. Gorbatov, V. T. Volkov, C. Journet, and M. Burghard, Science **284**, 1508 (1999).

[12] M. Tinkham, *Introduction to Superconductivity* (McGraw-Hill, New York, 1996), p. 201, ISBN 0-07-064878-6.

[13] A. F. Morpurgo, J. Kong, C. M. Marcus, and H. Dai, Science **286**, 263 (1999).

[14] M. R. Buitelaar, W. Belzig, T. Nussbaumer, B. Babic, C. Bruder, and C. Schönenberger, Phys. Rev. Lett. **91**, 057005 (2003).

[15] M. R. Buitelaar, T. Nussbaumer, and C. Schönenberger, Phys. Rev. Lett. **89**, 256801 (2002).

[16] J. Kong, H. T. Soh, A. M. Cassell, C. F. Quate, and H. Dai, Nature (London) **395**, 878 (1998).

[17] K. Grove-Rasmussen, H. I. Jørgensen, and P. E. Lindelof, cond-mat/0601371.

[18] A. F. Andreev, Sov. Phys. JETP **19**, 1228 (1964).

[19] G. E. Blonder, M. Tinkham, and T. M. Klapwijk, Phys. Rev. B **25**, 4515 (1982).

[20] T. M. Klapwijk, G. E. Blonder, and M. Tinkham, Physica (Amsterdam) **109B+C–110B+C**, 1657 (1982).

[21] P. E. Gregers-Hansen, E. Hendricks, M. T. Levinsen, and G. R. Pickett, Phys. Rev. Lett. **31**, 524 (1973).

[22] M. Octavio, M. Tinkham, G. E. Blonder, and T. M. Klapwijk, Phys. Rev. B **27**, 6739 (1983).

[23] J. C. Cuevas and W. Belzig, Phys. Rev. B **70**, 214512 (2004).

[24] A. Martín-Rodero, A. Levy Yeyati, and J. C. Cuevas, Superlattices Microstruct. **25**, 925 (1999).

[25] J. C. Cuevas, A. Martín-Rodero, and A. L. Yeyati, Phys. Rev. B **54**, 7366 (1996).

[26] V. S. Shumeiko, E. N. Bratus, and G. Wendin, Low Temp. Phys. **23**, 181 (1997).

[27] E. Vecino, M. R. Buitelaar, A. Martín-Rodero, C. Schönenberger, and A. L. Yeyati, Solid State Commun. **131**, 625 (2004).

[28] P. Joyez, P. Lafarge, A. Filipe, D. Esteve, and M. H. Devoret, Phys. Rev. Lett. **72**, 2458 (1994).

[29] The important parameter for the validity of this description is the quality factor $Q > 1$, which is estimated following Ref. [9] to be larger than 2 in our case, with $C = 4$ pF, $C_J = 1$ fF, $R = 6\ \Omega$, $R_J = 10\ \text{k}\Omega$, and $I_C = 35$ nA.